Received: 21 October 2024 | Revised: 15 December 2024 | Accepted: 10 February 2025

DOI: 10.1096/fba.2024-00190

RESEARCH ARTICLE

FASEB BioAdvances WILEY

Tumor innervation in cervical cancer: Prognostic insights from myelin-associated risk signatures

Guoqiang Chen[1] | **Zhen Zheng**[2] | **Qingqing Ji**[3] | **Ruihua He**[4] | **Zhouyuan Pan**[1] | **Yunxia Chen**[1] | **Yuqing Zhou**[1] | **Zhihong Wei**[1] | **Hao Sun**[5] | **Lixia Feng**[1]

[1]Department of Gynecology, The People's Hospital of Baoan Shenzhen, The Second Affiliated Hospital of Shenzhen University, Shenzhen, China

[2]Department of Obstetrics and Gynecology, National Clinical Research Centre for Obstetric and Gynecologic Diseases, Peking Union Medical College Hospital, Chinese Academy of Medical Sciences and Peking Union Medical College, Beijing, China

[3]Department of Anesthesiology, Shidong Hospital Affiliated to University of Shanghai for Science and Technology, Shanghai, China

[4]Department of Pharmacy, Shanghai Fourth People's Hospital, School of Medicine, Tongji University, Shanghai, China

[5]Department of Obstetrics and Gynecology, Shanghai Changzheng Hospital of Naval Medical University, Shanghai, China

Correspondence
Hao Sun, Department of Obstetrics and Gynecology, Shanghai Changzheng Hospital of Naval Medical University, 415 Fengyang Road, Huangpu District, Shanghai 200003, China.
Email: sunhao080011@163.com

Lixia Feng, Department of Gynecology, The People's Hospital of Baoan Shenzhen, The Second Affiliated Hospital of Shenzhen University, No. 118, Longjing 2nd Road, Xin'an Street, Bao'an District, Shenzhen 518100, China.
Email: fenglixia2000@sina.com

Abstract

The reported frequencies of perineural invasion (PNI) in human cervical cancer, ranging from 7.0% to 35.1%, may underestimate the significant role that nerves play in cervical cancer progression. Neurosecretory factors can promote tumor migration and invasion, even in cases classified as "PNI-negative". This study aimed to clarify whether tumor innervation influences tumor progression and cervical cancer patient outcomes. We first evaluated the gene signatures of human myelinating Schwann cells (SCs) using the Inferring Pathway Activity and Suppression (IPAS) scoring system to predict the degree of tumor innervation in 304 cervical cancer patients from The Cancer Genome Atlas (TCGA) database. Subsequently, we constructed a myelin-associated risk prognostic signature using LASSO regression analysis. Finally, we obtained a risk score using a quantitative formula and categorized all samples into high- and low-risk score groups. Our results indicated that tumor innervation in cervical cancer is associated with poor patient survival. Higher levels of innervation were correlated with an impaired immune response and reduced expression of immune checkpoints, including PD-L1. The prognostic model demonstrated

Abbreviations: AUC, areas under the time-dependent ROC curves; CESC, cervical squamous cell carcinoma and endocervical adenocarcinoma; C-index, concordance index; DEGs, differentially expressed genes; DFS, disease-free survival; GO, Gene Ontology; GSEA, Gene Set Enrichment Analysis; GSVA, Gene Set Variation Analysis; H&E, hematoxylin and eosin; IC_{50}, the half-maximal inhibitory concentration; ICIs, immune checkpoint inhibitors; IFN-γ, interferon-γ; IPAS, Inferring Pathway Activity and Suppression; KEGG, Kyoto Encyclopedia of Genes and Genomes; LASSO, least absolute shrinkage and selection operator; LVSI, lymphovascular space invasion; OS, overall survival; PFS, progression-free survival; PNI, perineural invasion; ROC, receiver operating characteristic; SCs, Schwann cells; ssGSEA, single-sample Gene Set Enrichment Analysis; TCGA, The Cancer Genome Atlas; TME, tumor microenvironment; TNF, tumor necrosis factor.

Guoqiang Chen, Zhen Zheng, Qingqing Ji, and Ruihua He contributed equally to this work.

excellent consistency between predicted and actual survival outcomes. Overall, tumor innervation plays a crucial role in regulating cervical cancer prognosis. The identified prognostic risk signatures offer a valuable tool for risk stratification and prognostic prediction in clinical practice.

KEYWORDS

cervical cancer, myelinating, prognosis, Schwann cells, tumor innervation

1 | INTRODUCTION

Neuronal development and communication pathways are significantly disrupted during tumorigenesis. Emerging evidence indicates that innervation within the tumor microenvironment (TME) exhibits a bidirectional and highly complex nature, extending beyond perineural invasion (PNI) and correlating with unfavorable clinical outcomes.[1] PNI is defined as tumor cells enveloping, infiltrating, and damaging neural structures, demonstrating the intimate interaction between malignant cells and nerves.[2,3] Notably, even in the absence of PNI, the mere proximity of tumor cells to nerves has been associated with poorer prognosis.[4] This suggests that neural involvement in tumor progression can manifest in "PNI-negative" cases without requiring direct physical contact between tumor cells and nerves.

Accumulating evidence demonstrates that tumor innervation actively drives cancer progression through multiple mechanisms.[5,6] Specifically, neurotrophic factors and neuropeptides secreted by neural components within the TME significantly enhance tumor cell proliferation, migration, and invasive capabilities.[7,8] Conversely, tumor cells reciprocally promote intratumoral innervation through the secretion of neurotrophic factors and tumor-derived exosomes, establishing a bidirectional communication network.[9,10] Moreover, neural-derived signaling molecules contribute to tumor progression by modulating the immune microenvironment, creating an immunosuppressive niche that facilitates tumor growth.[11,12] Supporting this concept, clinical and experimental studies have shown that denervation procedures can effectively inhibit tumor progression.[11,13] Based on these findings, we systematically investigated the clinical significance of tumor innervation by examining the correlation between innervation density and patient outcomes.

The concepts of "tumor innervation" and "nerve density" are often used interchangeably in the literature.[14] Quantification of innervation density is typically achieved through histological measurement of neural structures, expressed as either the number or area of nerves per mm^2 in the bulk tumor or tumor-adjacent stroma.[14] Given that myelination, a process mediated by Schwann cells (SCs), forms an essential structural component surrounding neural axons. Therefore, we employed human myelinating SCs signatures as a reliable biomarker to evaluate nerve density in cervical squamous cell carcinoma and endocervical adenocarcinoma (CESC) from The Cancer Genome Atlas (TCGA) database. Our comprehensive analysis aimed to elucidate the clinical significance of nerve density by investigating its associations with multiple parameters, including: (1) clinicopathological characteristics, (2) tumor immune microenvironment composition, (3) immune checkpoint expression profiles, and (4) chemotherapy response patterns in cervical cancer patients. Ultimately, we established a prognostic risk stratification model based on myelinating SCs-associated differentially expressed genes (DEGs), providing a novel tool for outcome prediction in cervical cancer management.

2 | METHOD DETAILS

2.1 | Clinical samples

Our study included 41 cervical cancer inpatients from the Department of Obstetrics and Gynecology, Shanghai Changzheng Hospital of Naval Medical University, between 01/01/2020 and 31/12/2020. Morphological evaluation and quantification of innervation and PNI were performed by a blinded pathologist using hematoxylin and eosin (H&E) staining. For immunofluorescence analysis, tissue sections were fixed with 4% paraformaldehyde, permeabilized, and blocked in 3% goat serum and 0.1% Triton X-100/PBS for 1 h. A rabbit anti-S100B primary antibody (Solarbio, K001720P) was used for immunofluorescence staining. The sections were then incubated overnight at 4°C with the primary antibody. Detection was performed using an Alexa Fluor 594-conjugated secondary antibody (ABclonal, AS039). Finally, the samples were mounted in mounting medium with DAPI and analyzed using a confocal microscope.

2.2 | Correlations between SCs gene signature scores and clinical outcomes in the TCGA cohort

SCs signatures were obtained from three primary sources: Tabula-Sapiens using OnClass[15] (http://tabula-sapiens-onclass.ds.czbiohub.org/), PanglaoDB,[16] and a single-cell analysis study conducted by Luca Tosti[17]. The recently developed Inferring Pathway Activity and Suppression (IPAS) scoring system was implemented to facilitate comparative analysis of SCs-related and other pathway activities across tumor samples[18] (https://github.com/RevaLab/PathwayAssessor). Corresponding clinical data, patient survival information, and raw genomic data of 304 CESC cases were retrieved from the TCGA database (https://portal.gdc.cancer.gov/). Cox regression analyses were employed to examine the correlation between SCs signature IPAS scores and patient outcomes. Optimal patient stratification based on IPAS scores was determined using the best cutoff method and visualized through an online bioinformatics platform (https://www.bioinformatics.com.cn). For subsequent exploratory analysis, patients were stratified into low- and high-score groups using a 10:90 distribution ratio.

2.3 | Correlations between SCs gene signature scores and clinicopathological characteristics in the TCGA cohort

The clinical and histopathological characteristics of patients with CESC were systematically analyzed and correlated with SCs signature IPAS scores. The analysis included the following clinicopathological parameters: histological subtype, tumor stage, PNI status, lymphovascular space invasion (LVSI), lymph node metastasis, and distant metastasis. Statistical comparisons were performed using Student's *t*-test, with a threshold of $p < 0.05$ considered statistically significant.

2.4 | Differential gene expression analysis and pathway enrichment analysis

Differential gene expression analysis was performed using the edgeR Bioconductor package (http://bioconductor.org/packages/edgeR/). Patient stratification was performed using a 10:90 distribution ratio, with the majority of cases assigned to the high SCs signature score group. Raw count data from these patients were extracted, and edgeR was used to identify DEGs between the two groups. The threshold for identifying DEGs was set at an absolute log2 (fold-change) ≥1.0 and $p < 0.05$. Functional enrichment analyses, including Gene Ontology (GO), Kyoto Encyclopedia of Genes and Genomes (KEGG) pathway analysis, and Gene Set Enrichment Analysis (GSEA), were performed to investigate pathway alterations in CESC using SCs signature IPAS scores as the primary classification criterion.

2.5 | Analysis of immune cell infiltration and immune checkpoint molecules

To investigate the impact of tumor innervation on immune cell infiltration within the TME, we systematically evaluated 28 distinct subpopulations of tumor-infiltrating leukocytes using established methodologies.[19] The relative abundance of each immune cell subtype was quantified through single-sample Gene Set Enrichment Analysis (ssGSEA) implemented in the Gene Set Variation Analysis (GSVA) R package. Furthermore, to elucidate the relationship between SCs gene signature scores and key immune checkpoint molecules, we identified and analyzed 18 clinically relevant immune checkpoint molecules based on a comprehensive literature review.[20,21]

2.6 | Sensitivity analysis of chemotherapy drugs

Chemotherapeutic drug sensitivity was predicted using the "pRRophetic" package (https://github.com/paulgeeleher/pRRophetic).[22] The half-maximal inhibitory concentration (IC_{50}) values, representing the drug concentration required to inhibit 50% of cancer cell proliferation, were used to quantify tumor sensitivity to each chemotherapeutic agent. The non-parametric Mann–Whitney U test was performed to compare the mean IC_{50} values for each drug between two patient groups.

2.7 | Establishment of a myelin-associated prognostic risk model

To identify prognostic genes in the TCGA-CESC cohort, we employed Least Absolute Shrinkage and Selection Operator (LASSO) regression analysis to avoid overfitting and eliminate closely related genes. Subsequently, a risk signature was further established based on the results from the multivariate Cox regression analysis. The formula for calculating the risk score was as follows:

$$\text{Risk score} = \Sigma \left[\text{Exp (gene)} \times \text{Coef (gene)}\right]$$

Here, Exp(gene) represents the gene expression level, and Coef(gene) denotes the regression coefficient. Based on the calculated risk scores, the samples were stratified into high-risk and low-risk groups using the median risk score as the cutoff. Survival analysis, receiver operating characteristic (ROC) curves, and the areas under the time-dependent ROC curves (AUC) were generated using the "survminer" and "survival" R packages. The prognostic risk signature was validated in both the training and testing cohorts.

2.8 | Development of a novel predictive nomogram

A nomogram integrating the risk score and other clinicopathological features was developed to provide a reliable tool for predicting the prognosis and overall survival of CESC patients at 1, 3, and 5 years. Each variable was assigned a score based on the point scale of the nomogram according to the coefficients of the logistic regression equation. By summing these scores, we estimated the prognosis of CESC patients. The accuracy of the predicted outcomes was evaluated using a calibration curve, which compared the predicted results with actual survival data. Additionally, the predictive accuracy of each variable was assessed using the concordance index (C-index).

2.9 | Statistical analysis

The source code for IPAS analysis is accessible on GitHub at https://github.com/RevaLab/PathwayAssessor. The R package for pRRophetic is available at https://github.com/paulgeeleher/pRRophetic. The external validation dataset was obtained from the GEO database (https://www.ncbi.nlm.nih.gov/geo/, accession ID: GSE44001). Kaplan–Meier survival curves, along with log-rank tests, were used to compare survival outcomes across different groups. The Mann–Whitney U test was used to compare chemotherapy drug sensitivity between the two groups, while Student's *t*-test was used for comparing continuous variables. All statistical analyses were performed using R software (v4.1.3). Statistical significance was defined as $p < 0.05$ in all analyses.

2.10 | Ethics statement

This study received ethical approval from the Ethics Committee of Shanghai Changzheng Hospital of Naval Medical University. All procedures involving human participants were conducted in accordance with the Declaration of Helsinki (1964) and its subsequent amendments. The human cervical cancer samples utilized in this research were obtained during routine radical hysterectomy procedures. Informed consent forms were obtained from all participating patients.

3 | RESULTS

3.1 | Myelinating SCs signature scores correlate with unfavorable survival in patients with cervical squamous cell carcinoma and endocervical adenocarcinoma

We first used OnClass to extract several human SCs signatures from the Tabula Sapiens portal,[15] including myelinating and non-myelinating SCs subtypes (Figure 1A). During SCs development, Schwann cell precursors differentiate into immature SCs, which subsequently mature into either myelinating or non-myelinating SCs. Notably, in response to nerve damage, myelinating SCs demonstrate plasticity by reverting to a non-myelinating state to facilitate nerve repair.[23] Terminal SCs, which envelop axon terminals, play a crucial role in mediating neural communication between the nervous system and peripheral tissues.[24] To investigate SCs signatures in CESC, we implemented a novel analytical approach, IPAS,[18] to calculate SCs signature scores based on gene expression profiles from 304 CESC patients in the TCGA database

FIGURE 1 Myelinating SCs signature scores correlate with unfavorable outcome in patients with cervical squamous cell carcinoma and endocervical adenocarcinoma. (A) Schematic representation of the hierarchical organization of SCs from the Tabula Sapiens dataset, with dashed arrows indicating transitions within the SCs lineage. (B–E) H&E and S100 staining were used to identify tumor cells and nerves. Tumor innervation was characterized by nerves located adjacent to, but not in direct contact with the tumor bulk edges (B, C). PNI was identified by nerves entrapped within the cervical squamous cell carcinoma tissues (D, E). Green dashed lines outline the nerves, while yellow dashed lines and the letter "C" mark the cervical cancer cells. Scale bar: 100 μm. (F, G) Kaplan–Meier curves depicting PFS and OS in 304 TCGA CESC patients stratified by high or low IPAS scores for myelinating SCs signatures, using the best cutoff stratification method. (H, I) Kaplan–Meier curves showing 5-year PFS and 5-year OS in 304 TCGA CESC patients stratified by high or low IPAS scores for myelinating SCs signatures, using the 10:90 ratio stratification method. (J) Univariate analysis evaluating the prognostic value of myelinating SCs signatures in TCGA CESC patients.

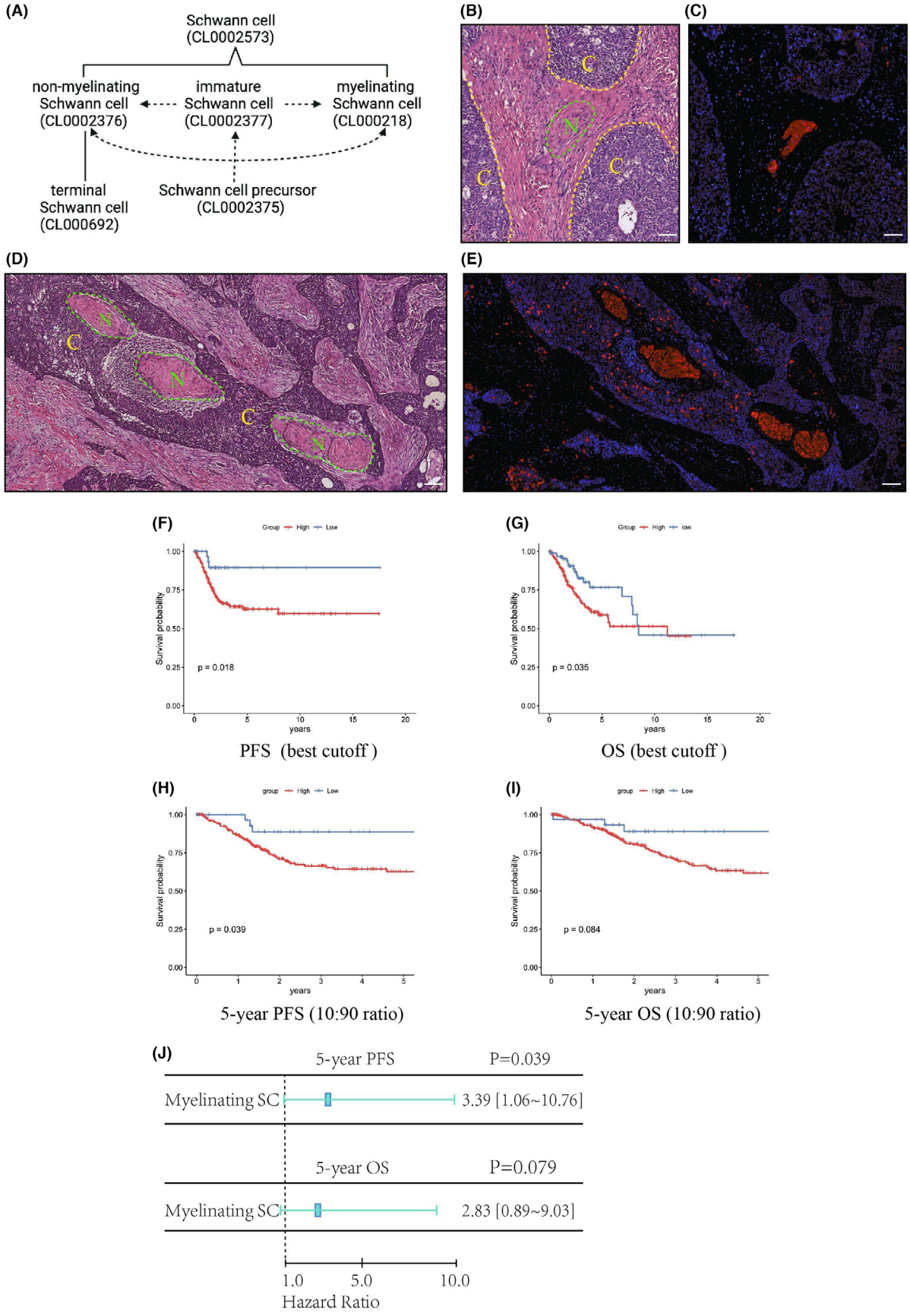
(A)
Schwann cell
(CL0002573)
non-myelinating
Schwann cell
(CL0002376)
immature
Schwann cell
(CL0002377)
myelinating
Schwann cell
(CL000218)
terminal
Schwann cell
(CL000692)
Schwann cell precursor
(CL0002375)
(B)
(C)
(D)
(E)
(F)
Group High Low
Survival probability
p = 0.018
years
PFS (best cutoff)
(G)
Group High low
p = 0.035
OS (best cutoff)
(H)
group High Low
p = 0.039
5-year PFS (10:90 ratio)
(I)
p = 0.084
5-year OS (10:90 ratio)
(J)
5-year PFS
P=0.039
Myelinating SC
3.39 [1.06~10.76]
5-year OS
P=0.079
2.83 [0.89~9.03]
1.0
5.0
10.0
Hazard Ratio

(Supplemental Material 1). We then examined the correlation between the SCs signature scores and patients' clinical outcomes. After applying the best cutoff stratification, we revealed a significant association between clinical outcomes and myelinating SCs signature scores, with higher scores correlating with poorer prognosis (Figure 1F,G). Following the methodological framework established by Sylvie Deborde et al.,[25] we stratified patients using a 10:90 ratio, assigning the majority to the high SCs signature group. This stratification demonstrated that elevated myelinating SCs signatures were significantly associated with reduced 5-year progression-free survival (PFS), with a parallel trend observed for 5-year overall survival (OS) (Figure 1H,I). Subsequent univariate Cox regression analysis confirmed the association between myelinating SCs scores and 5-year PFS, while the trend for 5-year OS did not reach statistical significance (Figure 1J).

3.2 | Integrated clinical characterization with myelinating SCs signature scores in patients with cervical squamous cell carcinoma and endocervical adenocarcinoma

The clinicopathological characteristics of patients in the TCGA dataset are summarized in Table 1. Our analysis revealed a significant association between myelinating SCs signature scores and histological subtypes, with adenocarcinoma demonstrating significantly higher scores compared to squamous cell carcinoma (0.07039 vs. 0.03294, $p=0.0074$). Furthermore, locally advanced and advanced CESC also exhibited higher signature scores relative to early CESC (0.05924 vs. 0.03234, $p=0.019$). However, no statistically significant differences were found in myelinating SCs signature scores when comparing groups based on LVSI ($p=0.95$), PNI ($p=0.34$), lymph node involvement ($p=0.29$), or distant metastasis ($p=0.06$).

TABLE 1 Patients characteristics by IPAS score in the TCGA database.

Characteristics	IPAS score (median, *n*)	*p**
Histological type		
Adenocarcinoma	0.070, $n=47$	0.007
Squamous carcinoma	0.033, $n=252$	
Lymphovascular space invasion		
No	0.036, $n=68$	0.954
Yes	0.031, $n=77$	
Perineural invasion		
No	0.041, $n=228$	0.337
Yes	0.036, $n=39$	
Stage		
IA1~IB2, II A1	0.032, $n=181$	0.019
IB3, II A2, II B~IVB	0.059, $n=116$	
Lymph nodes involvement		
No	0.026, $n=133$	0.287
Yes	0.037, $n=60$	
Distant metastasis		
No	0.029, $n=116$	0.063
Yes	0.067, $n=10$	

*Student's *t*-test.

3.3 | Myelinating SCs-related genes modulate signaling pathways in the tumor microenvironment

GO and KEGG pathway enrichment analyses indicated that the gene expression signature of myelinating SCs was positively correlated with multiple cancer-related migratory pathways in the TCGA dataset. These pathways encompassed fundamental biological processes such as cell–cell adhesion, MAPK signaling, chemokine signaling, and cytokine production (Figure 2A,B). Similarly, GSEA further confirmed that upregulated DEGs were predominantly enriched in neural-related pathways. These included protein–protein interactions at synapses, serotonin release, acetylcholine release, dopamine release, negative regulation of neuron differentiation, Schwann cell development, and bidirectional axonal transport mechanisms (Figure 2C). Conversely, negatively correlated gene sets were involved in immune regulatory pathways, including innate immune response, lymphocyte-mediated immunity, tumor necrosis factor (TNF) production, T cell receptor signaling, cell killing, and interferon-γ (IFN-γ) signaling (Figure 2D).

3.4 | Correlation of myelinating SCs signature scores and the immune landscape

The tumor immune microenvironment plays a pivotal role in cervical cancer progression and therapeutic response. As shown in Figure 2D, significant enrichment of immune-related pathways, particularly those involving T cell activation and TNF signaling, was observed in patients with low IPAS scores. These findings suggest that low myelinating SCs signature scores may serve as a potential biomarker for predicting immune status in CESC patients. To further investigate the immunological landscape, we performed ssGSEA to quantify immune cell infiltration within the TME. Comparative analysis revealed substantial differences in immune profiles

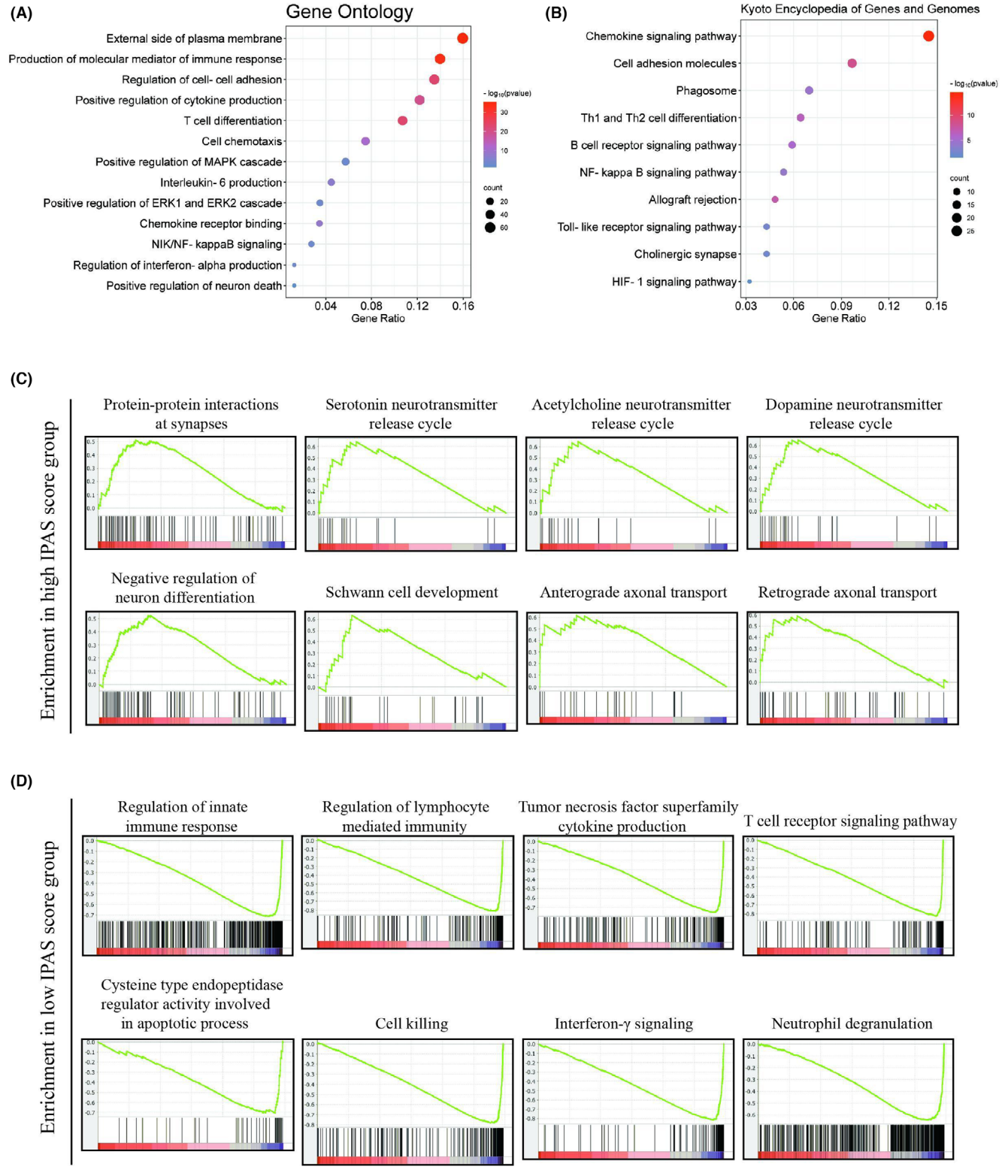

FIGURE 2 Myelinating SCs signature scores are associated with pathways related to cancer metastasis and impaired immune response. (A, B) GO and KEGG pathway enrichment analyses of upregulated DEGs in the high-IPAS score group. (C, D) GSEA was conducted on the expression profiles of the high-IPAS score group (C) and the low-IPAS score group (D), using pathway signatures from the GO, KEGG, and REACTOME databases.

between high and low IPAS score groups, with the high IPAS score group exhibiting marked reductions in 26 out of 28 immune cell populations, including B cells, natural killer cells, macrophages, and both CD8+ and CD4+ T cells (Figure 3A). Subsequent correlation analysis using TCGA data demonstrated significant inverse relationships

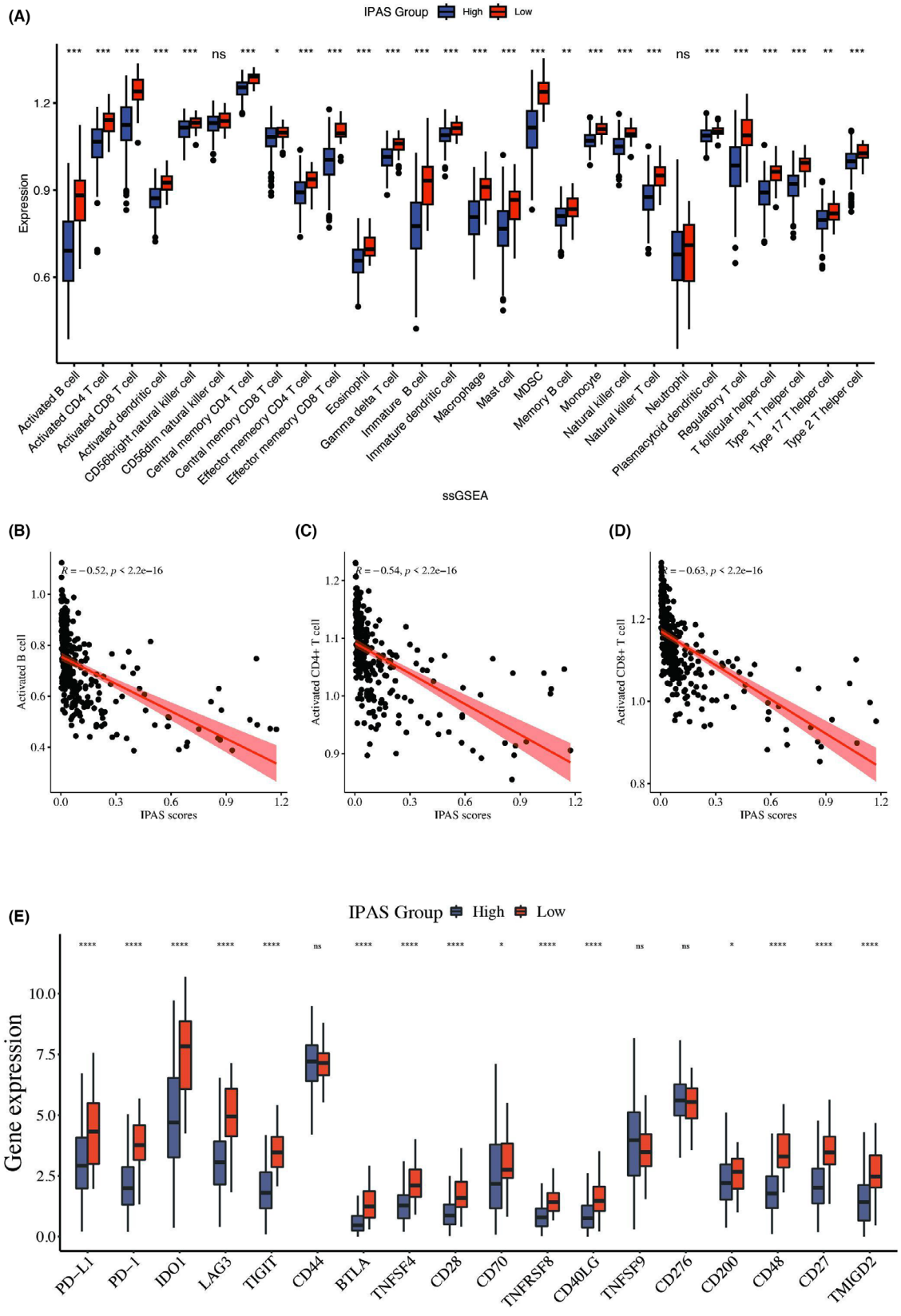

FIGURE 3 Association of myelinating SCs signature scores with the tumor immune microenvironment. (A) Abundance of 28 immune cell types in CESC patients stratified by high and low IPAS scores, as determined by the ssGSEA algorithm. (B–D) Pearson correlation analysis between myelinating SCs signature scores (IPAS scores) and the expression levels of B cells, CD4+ T cells, and CD8+ T cells in the TCGA dataset. (E) Differential expression of key immune checkpoint molecules between the high- and low-IPAS score groups.

between myelinating SCs signature scores and the infiltration levels of B cells, CD4+ T cells, and CD8+ T cells (Figure 3B–D). These collective results suggest enhanced anti-tumor immune activity in tumors with lower myelinating SCs signature scores.

Given the emerging role of immune checkpoint inhibitors (ICIs) in managing advanced and recurrent cervical cancer, we extended our analysis to examine the relationship between myelinating SCs signature scores and key immune checkpoint molecules. We systematically evaluated the expression patterns of 18 clinically relevant immune checkpoint markers, including PD-L1, PD-1, IDO1, LAG3, TIGIT, CD44, BTLA, TNFSF4, CD28, CD70, TNFRSF8, CD40LG, TNFSF9, CD276, CD200, CD48, CD27, and TMIGD2 (Figure 3E). The analysis revealed a consistent downregulation of nearly all examined immune checkpoint molecules in the high IPAS score group.

3.5 | Correlation of myelinating SCs signature scores with chemotherapy drug sensitivity

We assessed the sensitivity to various chemotherapy drugs between high- and low-IPAS score groups using the pRRophetic algorithm. The results showed that paclitaxel, mitomycin C, vinblastine, cytarabine, and axitinib were more effective in patients in the high-IPAS score group (Figure 4A,D–G). In contrast, patients with low IPAS scores showed greater therapeutic responsiveness to cisplatin, camptothecin, and dasatinib (Figure 4B,C,H). These findings suggest that IPAS scoring may serve as a potential predictive biomarker for chemotherapy selection in cervical cancer treatment.

3.6 | Development of a myelin-associated prognostic risk signature

Based on the results from univariate Cox regression analysis, LASSO regression analysis was employed to construct a myelin-associated prognostic risk signature (Figure 5A,B). Through this approach, four genes, *P2RY13, CHIT1, MAB21L3, and EREG, were* selected for further analysis. Multivariate Cox regression analysis was then used to identify the independent prognostic impact of these genes on OS in patients (Figure 5C). Among the identified genes, *P2RY13* and *CHIT1* were identified as protective factors, with higher expression levels significantly associated with favorable prognosis (Figure 5D–G). In contrast, *MAB21L3* and *EREG* were identified as risk factors, as their elevated expression correlated with poorer prognosis (Figure 5D,E,H,I). Using these four genes, we developed an optimized myelin-associated prognostic risk signature to predict clinical outcomes in CESC patients. The risk score for each patient was calculated using the following formula:

$$\begin{aligned}\text{Risk score} = {} & (-0.27626) \times \text{Exp}(P2RY13) + (-0.23260) \\ & \times \text{Exp}(CHIT1) + (0.22664) \times \text{Exp}(MAB21L3) \\ & + (0.24888) \times \text{Exp}(EREG).\end{aligned}$$

3.7 | Validation of a myelin-associated prognostic risk signature

Using the scoring formula mentioned above, we calculated the risk score for each CESC patient in the TCGA cohort (Supplemental Material 2). Based on these scores, patients were stratified into high- and low-risk groups. The distribution of risk scores, survival status, and expression levels of *P2RY13, CHIT1, MAB21L3*, and *EREG* are shown in Figure 6A. Notably, as the risk score increased, the mortality risk among CESC patients rose significantly, while survival time decreased. Compared to the low-risk group, patients with high myelin-associated risk scores exhibited worse PFS and OS (Figure 6B,C). Univariate analysis further confirmed that the myelin-associated risk score served as an independent prognostic factor for both PFS and OS (HR = 2.37 and 2.93, respectively; $p < 0.0001$; Figure 6D). These findings enabled the development of a robust myelin-associated risk prognosis scoring system, which demonstrated strong predictive accuracy, with $AUC_{1year} = 0.76$, $AUC_{2year} = 0.72$, $AUC_{3year} = 0.69$, $AUC_{4year} = 0.73$, $AUC_{5year} = 0.73$ (Figure 6E).

The GSE44001 dataset was used as an external validation cohort to validate the prognostic predictive capacity of the myelin-associated signature. Survival analysis indicated that the high-risk group exhibited significantly worse disease-free survival (DFS) in the GSE44001 cohort (Figure 6F). The AUCs for predicting 1-, 2-, 3-, 4-, and 5-year DFS rates were 0.56, 0.60, 0.59, 0.66, and 0.67, respectively (Figure 6G). Collectively, these results suggest that the myelin-associated risk prognostic signature is a reliable tool for stratifying patient outcomes and predicting survival in CESC.

3.8 | Identifying the predictive capability of myelin-associated prognostic risk signature

We evaluated the prognostic value of the myelin-associated risk signature across various clinical characteristics and developed a comprehensive nomogram incorporating these factors (Figure 7A). The results showed that the N stage,

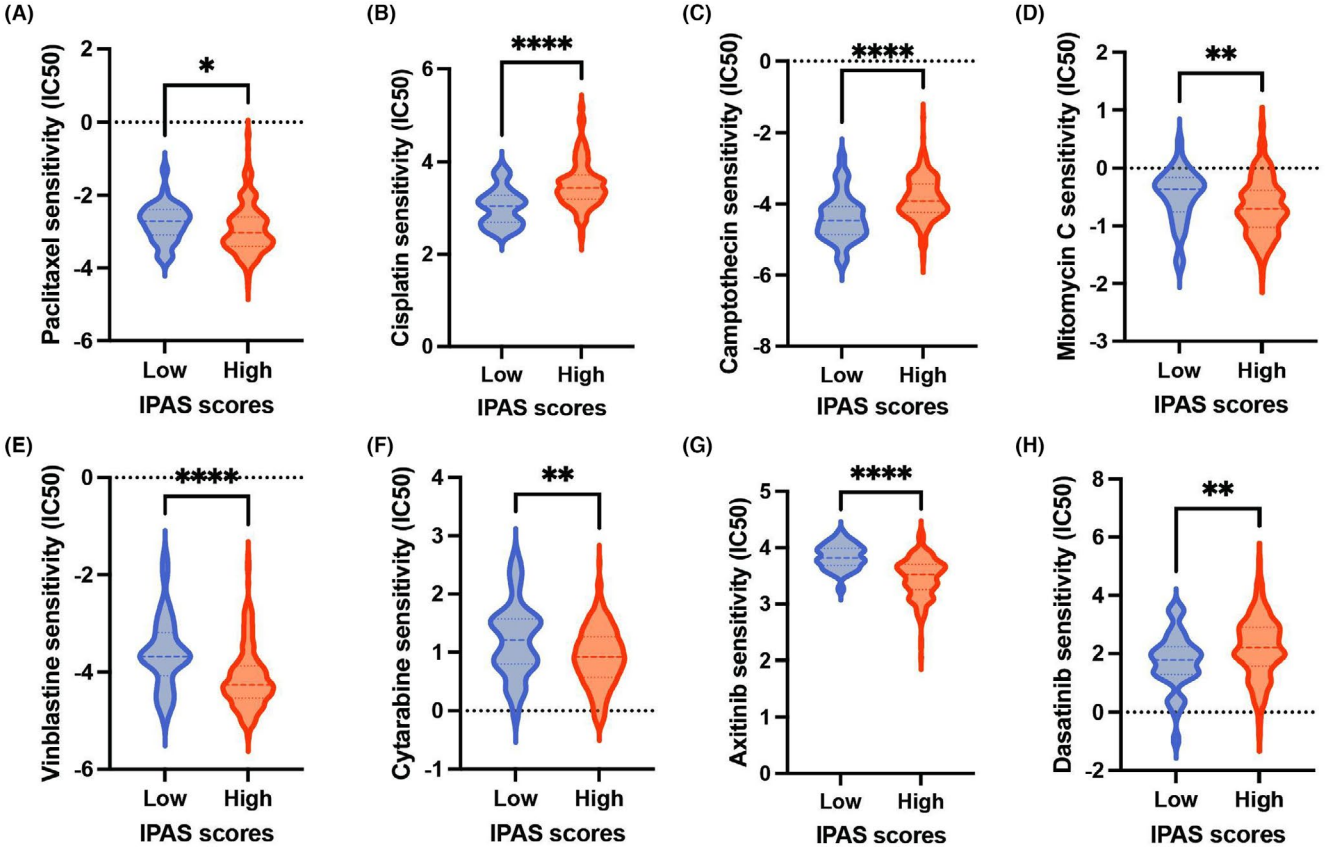

FIGURE 4 Association of myelinating SCs signature scores with chemotherapy drug sensitivity. (A–H) Boxplots displaying the predicted sensitivity to common chemotherapy drugs in cervical cancer patients, stratified by high- and low-IPAS score groups. Drug sensitivity is quantified using IC_{50} values, with the IC_{50} as the outcome variable.

T stage, and myelin-associated risk score significantly contributed to the prognostic model. Calibration curves for the nomogram indicated excellent agreement between predicted and observed survival probabilities, demonstrating the model's reliability (Figure 7B). Furthermore, the C-index analysis confirmed that the myelin-associated risk score exhibited the strongest predictive performance for OS among all evaluated parameters (Figure 7C).

4 | DISCUSSION

Mounting experimental evidence has demonstrated active nerve-tumor interactions in various cancers, including breast, pancreatic, oral, and colon cancers.[6,26–28] Despite significant advances in cancer neuroscience, the role of tumor innervation in cervical cancer remains poorly understood. Notably, the cervix is richly innervated,[29] yet the reported incidence of PNI in cervical cancer varies widely, ranging from 7.0% to 35.1%.[30] This variability suggests that conventional PNI assessments may overlook nerve-tumor interactions in patients classified as "PNI-negative". Myelinating SCs offer a potential indirect measure of nerve density; however, their detection in the TME remains challenging using traditional methods. To address this, we conducted a comprehensive bioinformatics analysis of gene expression profiles related to human myelinating SCs signatures in cervical cancer using data from the TCGA cohort.

Our computational analysis of TCGA data underscores the clinical relevance of myelinating SCs in CESC. High myelinating SCs scores were strongly associated with poor patient survival and emerged as robust prognostic indicators. Additionally, elevated myelinating SCs scores were more prevalent in adenocarcinoma subtypes and advanced-stage cervical cancer. Functional enrichment analysis revealed that myelinating SCs are linked to cancer invasion pathways (e.g., cell adhesion and cytokine/chemokine signaling) and neurotransmitter release (e.g., serotonin, acetylcholine, and dopamine). Intriguingly, T cell density decreased with tumor progression, and myelinating SCs were associated with immune suppression, characterized by impaired T cell signaling and reduced production of TNF and IFN-γ. Immune infiltration analysis revealed a near-complete depletion of immune cells in tumors with high myelinating SCs scores. Recent studies suggest that acetylcholine signaling reduces CD8+ T and Th1 cells while increasing Th2 cells and directly inhibiting

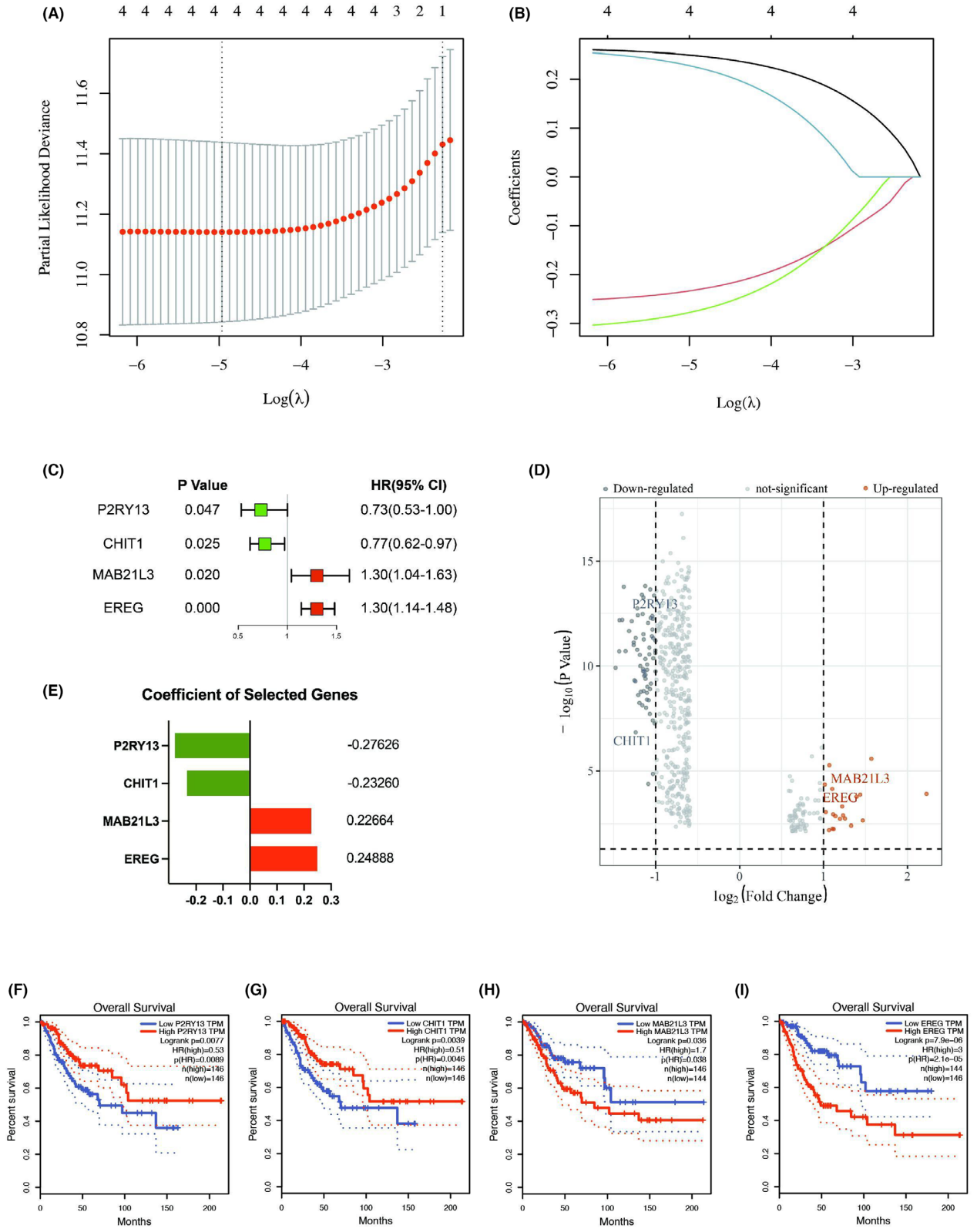

FIGURE 5 Establishment of a myelin-associated risk model for cervical cancer patients from the TCGA database. (A) Cross-validation plot for the penalty term. (B) LASSO regression analysis plot of the four DEGs. (C) Forest plot of the four DEGs identified by LASSO analysis. Red font indicates high risk associated genes, while green font indicates low risk associated genes. (D) Volcano plot displaying 86 DEGs with $|\log2FC| > 1$ and p-value < 0.05. Pink dots represent upregulated genes, while blue dots represent downregulated genes. (E) Coefficients of the four selected genes in the risk model. (F–I) Kaplan–Meier curves of the four myelinating SCs signature-associated genes for cervical cancer patients in the TCGA database.

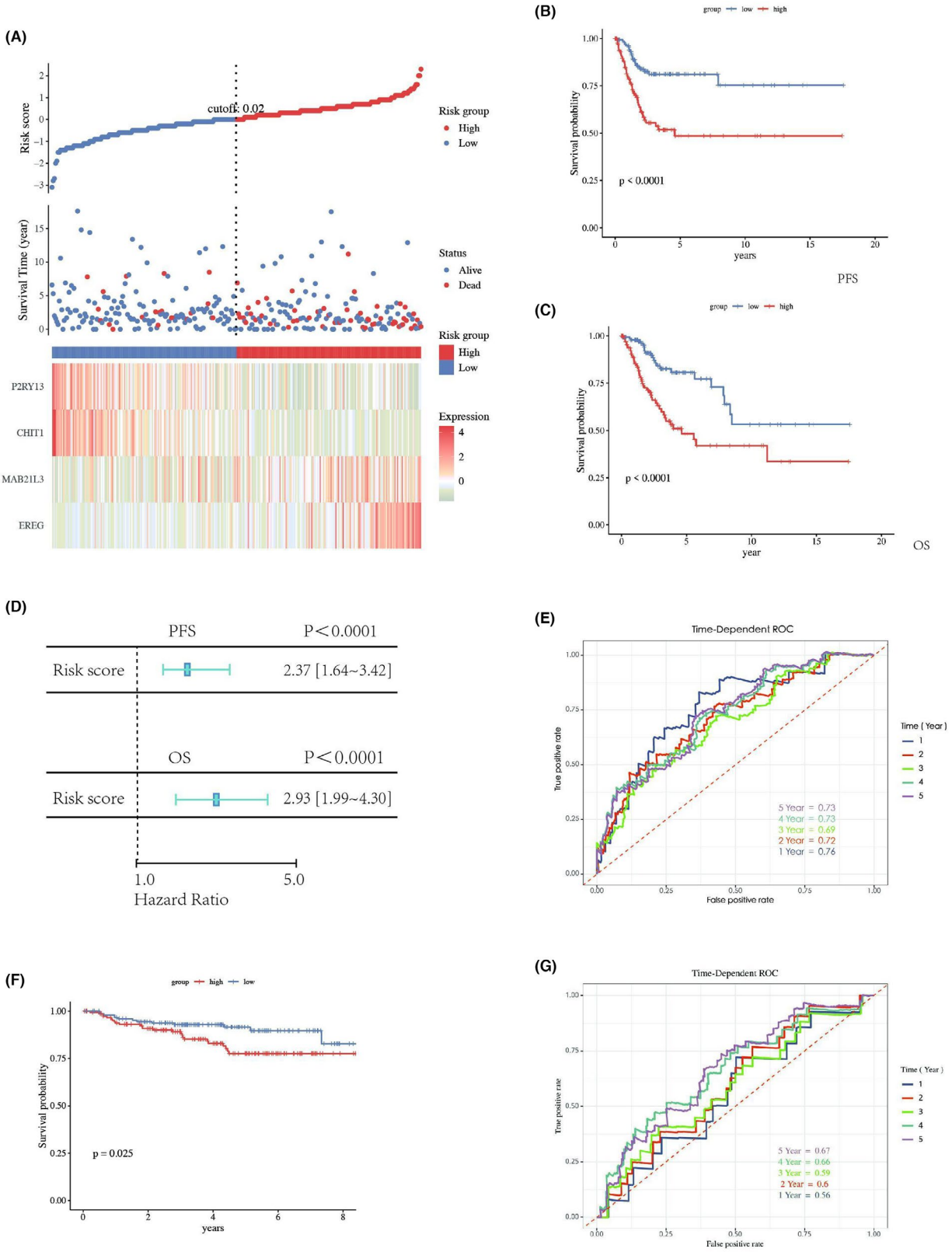

FIGURE 6 Validation of the myelin-associated risk prognostic signature. (A) Distribution of risk score, survival status, and expression levels of core myelinating SCs signature-associated genes contributing to risk score formation. (B, C) Kaplan–Meier curves comparing PFS (B) and OS (C) between low- and high-risk score groups in the TCGA cohort. (D) Univariate Cox regression analysis of risk score in the TCGA cohort. (E) AUC values of the ROC curve for risk score in the TCGA cohort. (F) Kaplan–Meier curves comparing DFS between low- and high-risk score groups in the GSE44001 cohort (external validation cohort). (G) AUC values of the ROC curve for risk score in the GSE44001 cohort.

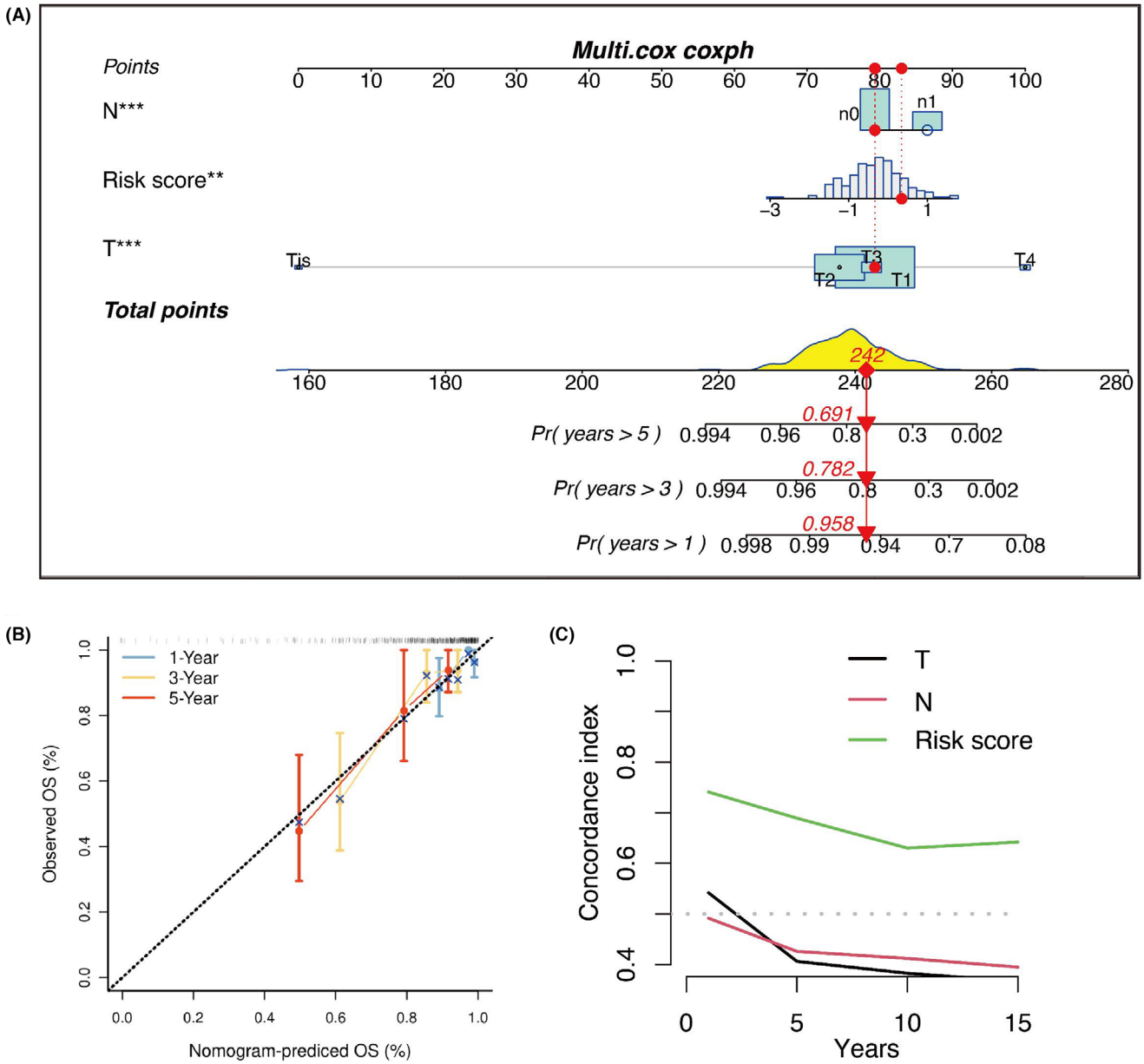

FIGURE 7 Evaluation of the predictive capability of the myelin-associated risk prognostic signature. (A) Establishment of a nomogram based on the myelin-associated risk prognostic signature to predict 1-, 3-, and 5-year OS in cervical cancer patients. (B) Calibration curves showing the consistency between predicted and observed 1-, 3-, and 5-year OS. (C) The C-index indicated that the risk score exhibited the strongest predictive performance for OS compared to other clinicopathological variables.

IFN-γ production.[11] Similarly, serotonin signaling contributes to immune evasion.[31,32] In our research, the reduced abundance of CD8+ T cells and diminished IFN-γ and innate immune responses in the high IPAS score group may explain the poorer outcomes observed in CESC patients with high tumor innervation. Furthermore, analysis of immune checkpoint molecules revealed higher expression of PD-L1, PD-1, IDO1, LAG3, TIGIT, BTLA, CD28, and CD27 in the low IPAS score group, suggesting that immunotherapy may be more effective in patients with low tumor innervation. Given that PD-1, a transmembrane protein on T cells, binds to overexpressed PD-L1 on tumor cells to induce immunosuppression,[20] our findings suggest that pembrolizumab and nivolumab may offer greater immunotherapeutic benefits for CESC patients with low tumor innervation.

To further explore the role of myelinating SCs, we identified myelinating SCs-associated genes using TCGA data. By integrating DEGs, we constructed a prognostic risk signature based on four genes (*P2RY13, CHIT1, MAB21L3, and EREG*) using Cox and LASSO regression analyses. This signature significantly correlated with OS in cervical cancer patients and was validated using an external GEO cohort, which revealed promising results,

indicating that these gene signatures are valuable candidates for tumor pathogenesis. Previous studies have implicated EREG in tumor metastasis, drug resistance, and cancer stemness.[33] Shengming Xu et al. found that EREG mediates PD-L1 upregulation and immune evasion via the EGFR-c-Myc pathway in head and neck squamous cell carcinoma.[34] Moreover, EREG is associated with the TGF-β signaling pathway[35] and serves as a risk factor for poor prognosis in cervical cancer.[36,37] MAB21L3 has been hypothesized to function as a transcriptional regulator influencing cell fate specification.[38] In contrast, *P2RY13* and *CHIT1* negatively regulate tumor innervation. High P2RY13 expression correlates with increased immune cell infiltration in the TME and favorable prognosis,[39,40] while also suppressing neuronal differentiation.[41] CHIT1-positive microglia contribute to motor neuron aging in the spinal cord.[42,43] Thus, the protective effects of *P2RY13* and *CHIT1* may stem from their roles in inhibiting neuronal differentiation and promoting neuronal aging. In our prognostic signature, *EREG* and *MAB21L3* acted as positive predictors, whereas *P2RY13* and *CHIT1* served as negative predictors of survival. Kaplan–Meier survival analysis confirmed that higher risk scores were associated with worse prognosis, suggesting that patients in the high-risk group likely exhibit greater tumor innervation.

To address the limitations of single biomarkers, we developed a nomogram integrating risk scores with tumor stage, which validated the predictive accuracy and clinical utility of our risk model. In conclusion, our results demonstrate that the myelinating SCs-based risk model effectively predicts CESC patient prognosis, with the risk score outperforming traditional N and T stages.

Our study has some limitations. First, the raw genomic data and corresponding clinical information were extracted from TCGA and GEO databases. Incorporating whole-slide histopathology images from TCGA could provide a more robust assessment of tumor innervation. However, manual quantification of all nerves within the tumor bulk and tumor-adjacent stroma using routine H&E staining is labor-intensive, and the staining quality of some TCGA images is suboptimal. Second, the molecular mechanisms underlying nerve-tumor interactions and associated genes in cervical cancer require further investigation.

In summary, tumor innervation represents a promising prognostic parameter in cervical cancer. To our knowledge, this is the first study to establish tumor innervation as a prognostic marker for cervical cancer. Our myelinating SCs-based risk model not only predicts patient outcomes but also opens new avenues for research into the mechanisms of tumor innervation and its potential as a therapeutic target in cervical cancer.

AUTHOR CONTRIBUTIONS

Guoqiang Chen designed the study, performed bioinformatics analysis, and prepared the manuscript. Zhen Zheng, Qingqing Ji, and Ruihua He retrieved the literature and revised the manuscript. Zhouyuan Pan, Yunxia Chen, Yuqing Zhou, and Zhihong Wei participated in the discussion and provided suggestions. Hao Sun and Lixia Feng conceived and supervised the research and provided critical review.

ACKNOWLEDGMENTS

N/A.

FUNDING INFORMATION

This work was supported by grants from the Medical and Health Research Project of the Medical Association of Baoan Shenzhen (BAYXH2023001 to Guoqiang Chen), the Medical and Health Basic Research Project of the Science and Technology Innovation Bureau of Baoan Shenzhen (2019JD078 to Lixia Feng), and the Science, Technology and Innovation Commission of Shenzhen Municipality (JCYJ20190809105003741 to Lixia Feng).

CONFLICT OF INTEREST STATEMENT

The authors have no conflict of interest.

DATA AVAILABILITY STATEMENT

All relevant data are within the manuscript and its additional files.

ETHICS APPROVAL AND CONSENT TO PARTICIPATE

This study involving human participants was approved by the Ethics Committee of Shanghai Changzheng Hospital, Naval Medical University. An informed consent form was obtained from all participants.

ORCID

Guoqiang Chen https://orcid.org/0000-0001-8555-9935
Lixia Feng https://orcid.org/0000-0003-0534-1288

REFERENCES

1. Reavis HD, Chen HI, Drapkin R. Tumor innervation: cancer has some nerve. *Trends Cancer*. 2020;6(12):1059-1067.
2. Meinel A, Fischer U, Bilek K, Hentschel B, Horn LC. Morphological parameters associated with perineural invasion (PNI) in carcinoma of the cervix uteri. *Int J Surg Pathol*. 2011;19(2):159-163.
3. Chen G, Sun H, Chen Y, et al. Perineural invasion in cervical cancer: a hidden trail for metastasis. *Diagnostics (Basel)*. 2024;14(14):1517.
4. Schmitd LB, Beesley LJ, Russo N, et al. Redefining perineural invasion: integration of biology with clinical outcome. *Neoplasia*. 2018;20(7):657-667.

5. Schmitd LB, Perez-Pacheco C, D'Silva NJ. Nerve density in cancer: less is better. *FASEB Bioadv*. 2021;3(10):773-786.
6. Li D, Hu LN, Zheng SM, et al. High nerve density in breast cancer is associated with poor patient outcome. *FASEB Bioadv*. 2022;4(6):391-401.
7. He S, Chen CH, Chernichenko N, et al. GFRalpha1 released by nerves enhances cancer cell perineural invasion through GDNF-RET signaling. *Proc Natl Acad Sci USA*. 2014;111(19):E2008-E2017.
8. Scanlon CS, Banerjee R, Inglehart RC, et al. Galanin modulates the neural niche to favour perineural invasion in head and neck cancer. *Nat Commun*. 2015;6:6885.
9. Allen JK, Armaiz-Pena GN, Nagaraja AS, et al. Sustained adrenergic signaling promotes intratumoral innervation through BDNF induction. *Cancer Res*. 2018;78(12):3233-3242.
10. Lucido CT, Wynja E, Madeo M, et al. Innervation of cervical carcinoma is mediated by cancer-derived exosomes. *Gynecol Oncol*. 2019;154(1):228-235.
11. Yang MW, Tao LY, Jiang YS, et al. Perineural invasion reprograms the immune microenvironment through cholinergic signaling in pancreatic ductal adenocarcinoma. *Cancer Res*. 2020;80(10):1991-2003.
12. Muthuswamy R, Okada NJ, Jenkins FJ, et al. Epinephrine promotes COX-2-dependent immune suppression in myeloid cells and cancer tissues. *Brain Behav Immun*. 2017;62:78-86. doi:10.1016/j.bbi.2017.02.008
13. Zhao CM, Hayakawa Y, Kodama Y, et al. Denervation suppresses gastric tumorigenesis. *Sci Transl Med*. 2014;6(250):250ra115. doi:10.1126/scitranslmed.3009569
14. Perez-Pacheco C, Schmitd LB, Furgal A, et al. Increased nerve density adversely affects outcome in Oral cancer. *Clin Cancer Res*. 2023;29(13):2501-2512.
15. Wang S, Pisco AO, McGeever A, et al. Leveraging the cell ontology to classify unseen cell types. *Nat Commun*. 2021;12(1):5556.
16. Franzen O, Gan LM, Bjorkegren JLM. PanglaoDB: a web server for exploration of mouse and human single-cell RNA sequencing data. *Database (Oxford)*. 2019;2019:ba.
17. Tosti L, Hang Y, Debnath O, et al. Single-nucleus and in situ RNA-sequencing reveal cell topographies in the human pancreas. *Gastroenterology*. 2021;160(4):1330-1344. e11.
18. Reva B, Omelchenko T, Calinawan A, Nair S, Schadt E, Tewari A. Prioritization of prostate cancer to immune checkpoint therapy by ranking tumors along IFN-γ axis and identification of immune resistance mechanisms. *bioRxiv [Internet]*. 2020. doi:10.1101/2020.10.19.345629v2.abstract
19. Charoentong P, Finotello F, Angelova M, et al. Pan-cancer immunogenomic analyses reveal genotype-immunophenotype relationships and predictors of response to checkpoint blockade. *Cell Rep*. 2017;18(1):248-262.
20. Xie Y, Kong W, Zhao X, Zhang H, Luo D, Chen S. Immune checkpoint inhibitors in cervical cancer: current status and research progress. *Front Oncol*. 2022;12:984896.
21. Zheng JH, Yao HF, Duan ZH, et al. Exploitation and verification of a stroma- and metastasis-associated risk prognostic signature in pancreatic adenocarcinoma. *Pharmaceuticals (Basel)*. 2022;15(11):1336.
22. Geeleher P, Cox N, Huang RS. pRRophetic: an R package for prediction of clinical chemotherapeutic response from tumor gene expression levels. *PLoS One*. 2014;9(9):e107468.
23. Jessen KR, Mirsky R, Lloyd AC. Schwann cells: development and role in nerve repair. *Cold Spring Harb Perspect Biol*. 2015;7(7):a020487.
24. Hastings RL, Valdez G. Origin, identity, and function of terminal Schwann cells. *Trends Neurosci*. 2024;47(6):432-446.
25. Deborde S, Gusain L, Powers A, et al. Reprogrammed Schwann cells organize into dynamic tracks that promote pancreatic cancer invasion. *Cancer Discov*. 2022;12(10):2454-2473.
26. Tian Z, Ou G, Su M, et al. TIMP1 derived from pancreatic cancer cells stimulates Schwann cells and promotes the occurrence of perineural invasion. *Cancer Lett*. 2022;546:215863.
27. Schmitd LB, Perez-Pacheco C, Bellile EL, et al. Spatial and transcriptomic analysis of perineural invasion in Oral cancer. *Clin Cancer Res*. 2022;28(16):3557-3572.
28. He S, He S, Chen CH, et al. The chemokine (CCL2-CCR2) signaling axis mediates perineural invasion. *Mol Cancer Res*. 2015;13(2):380-390.
29. Pinsard M, Mouchet N, Dion L, et al. Anatomic and functional mapping of human uterine innervation. *Fertil Steril*. 2022;117(6):1279-1288.
30. Zhu Y, Zhang GN, Shi Y, Cui L, Leng XF, Huang JM. Perineural invasion in cervical cancer: pay attention to the indications of nerve-sparing radical hysterectomy. *Ann Transl Med*. 2019;7(9):203.
31. Jiang SH, Li J, Dong FY, et al. Increased serotonin signaling contributes to the Warburg effect in pancreatic tumor cells under metabolic stress and promotes growth of pancreatic tumors in mice. *Gastroenterology*. 2017;153(1):277-291. e19.
32. Chen L, Huang S, Wu X, He W, Song M. Serotonin signalling in cancer: emerging mechanisms and therapeutic opportunities. *Clin Transl Med*. 2024;14(7):e1750.
33. Cheng WL, Feng PH, Lee KY, et al. The role of EREG/EGFR pathway in tumor progression. *Int J Mol Sci*. 2021;22(23):12828.
34. Xu S, Wang H, Zhu Y, et al. Stabilization of EREG via STT3B-mediated N-glycosylation is critical for PDL1 upregulation and immune evasion in head and neck squamous cell carcinoma. *Int J Oral Sci*. 2024;16(1):47.
35. Nagy A, Munkacsy G, Gyorffy B. Pancancer survival analysis of cancer hallmark genes. *Sci Rep*. 2021;11(1):6047.
36. Yang S, Yang X, Li C. Integrated analysis of EREG expression, a gene associated with cervical cancer prognosis. *Am J Cancer Res*. 2023;13(10):4644-4660.
37. Li T, Feng R, Chen B, Zhou J. EREG is a risk factor for the prognosis of patients with cervical cancer. *Front Med (Lausanne)*. 2023;10:1161835.
38. Takahashi C, Kusakabe M, Suzuki T, Miyatake K, Nishida E. mab21-l3 regulates cell fate specification of multiciliate cells and ionocytes. *Nat Commun*. 2015;6:6017.
39. Wang J, Shi W, Miao Y, Gan J, Guan Q, Ran J. Evaluation of tumor microenvironmental immune regulation and prognostic in lung adenocarcinoma from the perspective of purinergic receptor P2Y13. *Bioengineered*. 2021;12(1):6286-6304.
40. Lin J, Wu C, Ma D, Hu Q. Identification of P2RY13 as an immune-related prognostic biomarker in lung adenocarcinoma: a public database-based retrospective study. *PeerJ*. 2021;9:e11319.
41. Yano S, Tsukimoto M, Harada H, Kojima S. Involvement of P2Y13 receptor in suppression of neuronal differentiation. *Neurosci Lett*. 2012;518(1):5-9.

42. Wang Z, Cai W, Song W. CHIT1-positive microglia act as culprits for spinal motor neuron aging. *Sci China Life Sci*. 2024;67(4):847-848.
43. Sun S, Li J, Wang S, et al. CHIT1-positive microglia drive motor neuron ageing in the primate spinal cord. *Nature*. 2023;624(7992):611-620.

SUPPORTING INFORMATION

Additional supporting information can be found online in the Supporting Information section at the end of this article.

How to cite this article: Chen G, Zheng Z, Ji Q, et al. Tumor innervation in cervical cancer: Prognostic insights from myelin-associated risk signatures. *FASEB BioAdvances*. 2025;7:e70004. doi:10.1096/fba.2024-00190